

New Understanding on Relationship Between RTD Curve and Inclusion Behavior in the Tundish



CHANGYOU DING, HONG LEI, HAN ZHANG, YUANYOU XIAO, YAN ZHAO,
and ZONGSHU ZOU

The inclusion behavior depends on the turbulent flow in the tundish. To make a deep understanding on the relation between flow field and inclusion behavior, the residence time distribution (RTD) curve is applied to analyze the flow field, the inclusion mass/population conservation model is applied to explore the inclusion behavior, and Pearson correlation is introduced to investigate the relation of RTD curve and the inclusion coalescence-removal. The numerical flow field and the number density confirm well with the measured data. Among plug volume fraction, well-mixed volume fraction and dead volume fraction, dead volume fraction is the most important factor to affect the inclusion removal rate and the dimensionless inclusion characteristic radius. For the same control devices in a tundish, structure parameters (distance from dam/baffle to tundish exit, the diameter of the hole in the baffle) can be optimized to obtain the maximum inclusion removal rate. Such a critical state can be expressed by the ratio of plug volume fraction to well-mixed volume fraction. But the dimensionless characteristic radius may be the maximum or the minimum at this critical state.

<https://doi.org/10.1007/s11663-024-03087-1>

© The Minerals, Metals & Materials Society and ASM International 2024

I. INTRODUCTION

TO meet the demand of the modern industry, steel companies should produce more clean steel products. During the continuous casting process, tundish is not only a connector between the ladle and the mold, but also a refining reactor because there are some advanced metallurgical processes, such as plasma heating,^[1,2] induction heating,^[3,4] gas shroud technology^[5,6] in the tundish. The control of fluid flow and the inclusion removal are always two key issues that the tundish metallurgy has to face.

In the steelmaking factory, fluid flow is scarcely possible to approach because of high temperature environment. Therefore, metallurgists use mathematical model and water model to obtain residence time distribution (RTD) curve for analyzing the flow behavior in the tundish.^[7–10] Further, plug volume, dead volume and well-mixed volume in the tundish, which can be calculated by RTD curve, are applied to describe the fluid flow in the tundish. The values of these volumes are the indicators to optimize the tundish structure. For example, Wang *et al.* explored a kind of ceramic filter in the tundish,^[11] Huang *et al.* put forward a swirling chamber to produce the strong swirling flow in tundish,^[12] Chang *et al.* developed a type of gas curtain in a seven-strand tundish.^[13] Usually, the principle to optimize the tundish structure is that the smaller dead volume leads to a better tundish structure.

Inclusions collision-coalescence behavior is another essential issue. There are mainly two types of inclusion transport models: homogeneous model and non-homogeneous model. The non-homogeneous model, which comprises of Lagrange method^[14,15] and Euler method,^[16] is the most popular mathematical method. Lagrange model usually traces tens of thousands of inclusion particles, and Euler model divides the inclusion particles into several groups according to their size. It is very expensive to describe the inclusion behaviors accurately on the condition of current computational hardware.

CHANGYOU DING, HONG LEI, and HAN ZHANG are with the Key Laboratory of Electromagnetic Processing of Materials, Ministry of Education, Northeastern University, Shenyang 110819, Liaoning Province, P.R. China and also with the School of Metallurgy, Northeastern University, Shenyang 110819, Liaoning Province, P.R. China. Contact e-mail: leihong@epm.neu.edu.cn YUANYOU XIAO is with the Key Laboratory of Electromagnetic Processing of Materials, Ministry of Education, Northeastern University and also with the School of Materials and Metallurgy, University of Science and Technology Liaoning, Anshan 114051, Liaoning, P.R. China. YAN ZHAO and ZONGSHU ZOU are with the School of Metallurgy, Northeastern University.

Manuscript submitted January 26, 2024; accepted March 28, 2024.

Article published online April 24, 2024.

Some references indicate that the smaller dead volume fraction leads to the greater inclusion removal rate. However, some references point out that the smaller dead volume fraction doesn't represent the greater inclusion removal rate.^[15,17-21] In fact, there are some principles to optimize the tundish structure^[11-13,17]: (1) The greater plug volume fraction can promote the inclusion floatation. (2) The greater well-mixed volume fraction can promote the process of collision and aggregation for inclusions. (3) The smaller dead volume fraction can promote collision, coalescence and removal of inclusions. Among the three principles, only a few of papers studied the relationship between inclusion removal and plug/well-mixed volume fraction. For instance, Tkadleckova *et al.* designed an impact pad leading to the higher proportion of plug volume and the better inclusion removal efficiency;^[17] Yazdi *et al.* used a tall dam to increase the ratio of plug volume to dead volume and the ratio of well-mixed volume to dead volume in order to reach a higher inclusion removal ratio.^[22] Sheng *et al.* proposed the ratio of well-mixed volume to plug volume to be a new criterion to evaluate the inclusion removal.^[18]

In order to build a bridge between flow field and inclusion removal, the residence time distribution (RTD) curve is applied to analyze the character of flow field in the tundish, the inclusion mass/population conservation model is selected to explore the inclusion behavior, and Pearson correlation is introduced to investigate the relation of residence time distribution and the inclusion behavior. Meanwhile, water model experiment, industrial trial data and grid sensitivity are carried out to confirm the numerical result. Finally, relationship between RTD curve and inclusion coalescence-removal is investigated by a single-strand tundish and a two-strand tundish.

II. MATHEMATICAL DESCRIPTION

A. Basic Assumptions

The assumptions about complex metallurgical phenomena in the tundish are adopted as following:

- (1) The fluid in the tundish is considered as incompressible and Newtonian. And this paper doesn't consider the effect of non-isothermal temperature field and surface fluctuations on fluid flow in the tundish.^[11,15]
- (2) The shape of inclusion is spherical. Moreover, the continuous phase feature is applied in the inclusion phase.^[16,23]
- (3) The low inclusion volume concentration (< 500 ppm) makes the effect of the inclusion on the flow field can be neglected.^[24-26]
- (4) Inclusions are eliminated from the molten steel, when they come into contact with the slag blanket or refractory.^[24,25]

- (5) Brownian collision is negligible, because it is at least two orders less than turbulent collision.^[24,25]

B. Flow Field

The continuity equation and the momentum conservation equation are applied to describe the molten flow.

$$\nabla \cdot (\rho_f \mathbf{u}_f) = 0 \quad [1]$$

$$\nabla \cdot (\rho_f \mathbf{u}_f \mathbf{u}_f) = -\nabla p + \rho_f \mathbf{g} + \nabla \cdot (\mu_{\text{eff}} \nabla \mathbf{u}_f) \quad [2]$$

where \mathbf{u}_f is the velocity of molten steel, m/s; ρ_f is the density of molten steel, kg/m³; p is the pressure, Pa; μ_{eff} is the effective viscosity, Pa s.

The residence time distribution curve is calculated by the trace transfer equation.

$$\frac{\partial C_T}{\partial t} + \nabla \cdot (\mathbf{u}_f C_T) = \nabla \cdot (D_{\text{eff}} \nabla C_T) \quad [3]$$

where C_T is the tracer concentration; D_{eff} is the effective diffusion coefficient.

In order to analyze the flow behavior in the tundish, the classic combined method is applied.^[27,28] Table I gives the detail information about the different characteristic volume fraction in a tundish. It should be noted that the upper limit of integral can be calculated by the cut-off point: $C = C_0 + 5 \text{ pct}(C_{\text{max}} - C_0)$.^[27,28]

C. Inclusion Collision-Coalescence

Industrial trials show that the inclusion number density function decreases exponentially with the inclusion radius (r), $f(r) = A e^{-Br}$. Furthermore, the value of A and B are only related to the coordinates and the time.^[29-31] Therefore, the inclusion characteristic parameter [volume concentration (C), number density (N) and characteristic radius (r^*)] can be written as:

$$C = \int_0^{\infty} \frac{4}{3} \pi r^3 f(r) dr = 8\pi \frac{A}{B^4} \quad [4]$$

$$N = \int_0^{\infty} f(r) dr = \frac{A}{B} \quad [5]$$

$$r^* = \frac{\sqrt[3]{6}}{B} \quad [6]$$

The metallurgists have successfully employed the inclusion mass/population conservation model to calculate the inclusion behavior in some metallurgical reactors.^[23,32-34] The key governing equations of the inclusion transport can be written as follows.

Table I. RTD Curve Analysis Model

	Expression
Mean Residence Time	$\bar{t} = \frac{\int_0^\infty ct dt}{\int_0^\infty c dt}$
Dead Volume Fraction	$V_d = 1 - \frac{\bar{t}}{\tau}$
Plug Volume Fraction	$V_p = \frac{t_{\min} + t_{\max}}{2\tau}$
Well-Mixed Volume Fraction	$V_m = 1 - V_p - V_d$

where τ , t_{\min} and t_{\max} represent theoretical residence time, minimum residence time and peak concentration time, respectively.

$$\nabla \cdot (\mathbf{u}_C C) = \nabla \cdot (D_{\text{eff}} \nabla C) + S_C \quad [7]$$

$$\nabla \cdot (\mathbf{u}_N N) = \nabla \cdot (D_{\text{eff}} \nabla N) + S_N \quad [8]$$

where S_C is equal to 0.^[23,29] And S_N is the sum of turbulent collision (S_{turb}) and Stokes collision (S_{Stokes})^[23]:

$$S_N = S_{\text{turb}} + S_{\text{Stokes}} \quad [9]$$

$$\begin{aligned} S_{\text{turb}} &= \frac{1}{2} \int_0^\infty \int_0^\infty \alpha \beta_T(r_i, r_j) N_i N_j dr_i dr_j \\ &= 2.6\alpha \left(\frac{\pi \varepsilon}{\nu}\right)^{0.5} N^2 r^{*3} \end{aligned} \quad [10]$$

$$\begin{aligned} S_{\text{Stokes}} &= \frac{1}{2} \int_0^\infty \int_0^\infty \frac{2\pi g \Delta \rho}{9\mu} |r_i^2 - r_j^2| (r_i^2 + r_j^2) N_i N_j dr_i dr_j \\ &= \frac{10}{9\sqrt{3}} \frac{\pi g \Delta \rho}{\mu} N^2 r^{*4} \end{aligned} \quad [11]$$

where subscripts i and j are the correlation between radius r_i and r_j ; $\Delta \rho$ is the density difference. $\beta_T(r_i, r_j)$ is the collision rate of two particulates (r_i and r_j), m^3/s ; ν is kinematic viscosity, m^2/s ; ε is turbulent energy dissipation rate, m^2/s^3 ; N is inclusion number density, $1/\text{m}^3$; α is the coagulation coefficient as follows:

$$\alpha = 0.738 \left(\frac{\mu r^3 (\varepsilon/\nu)^{0.5}}{A_{\text{Hamaker}}} \right)^{-0.242} \quad [12]$$

where A_{Hamaker} is Hamaker constant for the inclusion in the steel.^[35]

The inclusion convection velocity (\mathbf{u}_C , \mathbf{u}_N) in Eqs. [7] and [8] consists of the velocity of fluid (\mathbf{u}_f) and the slip velocity between particle and fluid ($\mathbf{u}_{p,C}$, $\mathbf{u}_{p,N}$). The direction of the particle slip velocity is opposite to the gravitational acceleration. The detail expression can be found in Eqs. [13] through [16].

$$\mathbf{u}_C = \mathbf{u}_f + \mathbf{u}_{p,C} \quad [13]$$

$$\mathbf{u}_N = \mathbf{u}_f + \mathbf{u}_{p,N} \quad [14]$$

$$u_{p,C} = \frac{20c_1}{\sqrt[3]{36}} r^{*2} \quad [15]$$

$$u_{p,N} = \frac{2c_1}{\sqrt[3]{36}} r^{*2} \quad [16]$$

with

$$c_1 = \frac{2\Delta \rho g}{9\mu} \quad [17]$$

D. Boundary Condition

The inclusion characteristic parameter (number density and characteristic diameter) of molten steel are $4.50 \times 10^{13} \text{ m}^{-3}$, $2.27 \mu\text{m}$, respectively. Figure 1 shows inclusion adsorption locations in the tundish: slag and refractory. The convection and diffusion can be written as Eqs. [18] through [22].

$$\mathbf{F}_C^c = \mathbf{u}_{p,C} C \quad [18]$$

$$\mathbf{F}_N^c = \mathbf{u}_{p,N} N \quad [19]$$

$$\mathbf{F}_C^d = \left(\frac{16\pi}{3} \frac{C_2}{\sqrt[3]{6}} N r^{*4} \right) \cdot \mathbf{n} \quad [20]$$

$$\mathbf{F}_N^d = \left(\frac{C_2}{\sqrt[3]{6}} N r^{*4} \right) \cdot \mathbf{n} \quad [21]$$

with

$$C_2 = \frac{0.01\tau_0}{\rho \nu} \quad [22]$$

where \mathbf{n} is the unit vector; ρ is the density of molten steel; ν represents the kinematics viscosity of molten steel; τ_0 is the turbulent wall friction.

E. Physical Model and Solution Strategy

There are two types of tundishes in the present paper. Figure 2 shows the geometric model and the mesh system for the tundishes. Furthermore, the computational domains are discretized into 190 332 and 332 559

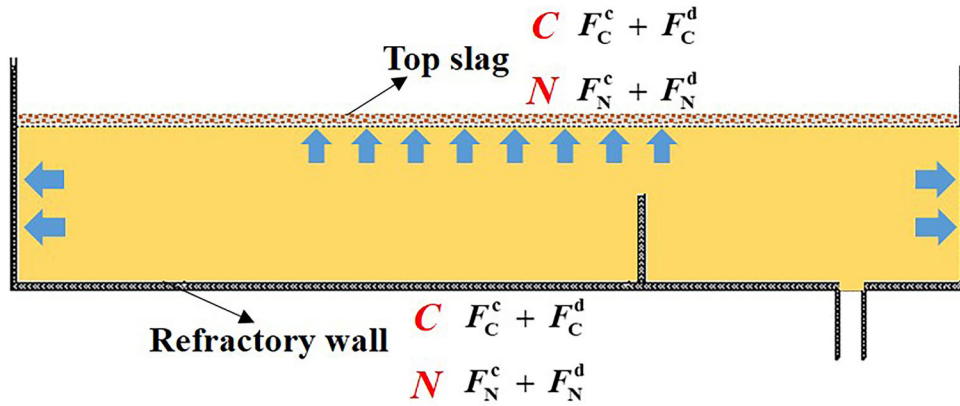


Fig. 1—Boundary conditions for the adsorption mechanism.

grids by ICEM CFD. Tables II and III gives tundish geometry size and detailed physical properties in the calculation.

Figure 3 shows the numerical procedure in the present research. All numerical procedures are arranged by the OpenFOAM-6.0. The solver *buoyantBoussinisqSimpleFoam* is used to describe the flow field. Based on solver *scalarTransportFoam*, we developed a transient solver *PerfectRTDFoam* to obtain the residence time distribution (RTD) curve. The inclusion mass/population conservation model is developed by C++ code. The solver is called *InclusionTransportFoam*. Furthermore, we use the *codedFixedValue* function to implement the boundary conditions.

III. SIMULATION VERIFICATION

A. Water Model

The water model experiment is conducted to restore the molten steel flow behavior in the tundish. The RTD curve is applied to analyze the flow field. The geometric parameters of water model are same as prototype tundish. The detail dimension can be acquired in our previous papers.^[36,37] Figure 4 shows that the numerical result has a good agreement with the water model experiment case. Mean residence time is the key parameter for RTD curve analysis. The differences of mean residence time between the predicted RTD curve and experimental RTD curve is only 3.6 pct. For peak concentration, the numerical simulation case only deviates 1.15 pct from the water model experiment case. However, the difference of peak concentration time between simulation and experiment is 23.33 pct. The tracer density and the tracer injected method may result in the error of peak concentration time.^[19]

B. Industrial Measurement

Based on Ling's paper,^[38] the samples are acquired from a 35t two-strand tundish, which geometry size is same as the two-strand tundish in Figure 2. The detailed physical properties can be found in Table III. The samples are detected and analyzed for number density

and the diameter distribution by using SEM-EDS system. Figure 5 lists the predicted inclusion number density and the industrial experimental data.^[38] When $d_{\text{inclusion}} > 15.5 \mu\text{m}$ and $15.63 \mu\text{m}$ at the ladle shroud and the tundish exit, numerical result has an obvious difference compared with measurement data. Several elements result in the differences: (1) The inclusion number density and the inclusion radius are considered as an exponential relation in the present numerical simulation. (2) In two-dimensional inclusion analysis, several small inclusions comprise a cluster inclusion. Actually, the inclusion is considered as a spatial structure in the mathematical model. (3) In the actual production, big inclusions in the molten steel maybe come from slag and refractory, but these factors are not considered in present numerical simulation.

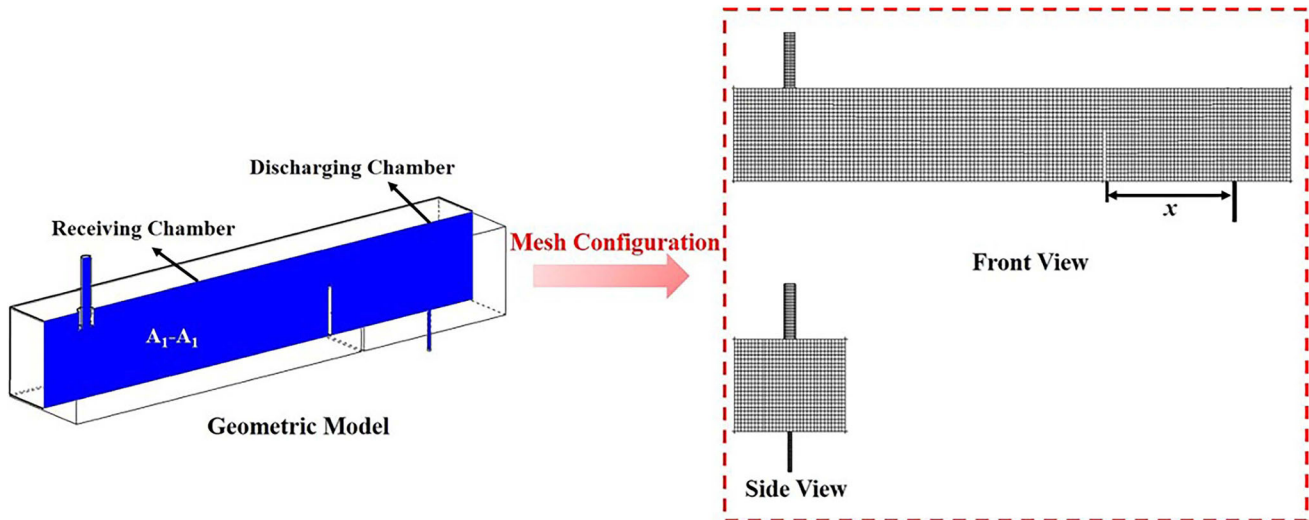
C. Grid Independence Verification

The inclusion behavior in the case of different grid numbers has been carried out in order to validate the numerical result. Figure 6 shows the inclusion characteristic parameter at the outlet under the condition of different grid numbers. When the single-strand tundish grid is refined from 190,332 to 291,132, the maximum difference is only 0.06 pct. When the two-strand tundish grid is refined from 332,559 to 495,457, the maximum difference is only 0.26 pct. The difference is only at least fourth significant digit. Therefore, the grid numbers (190,332 and 332,559) are chosen to conduct the simulation for reducing the calculation time.

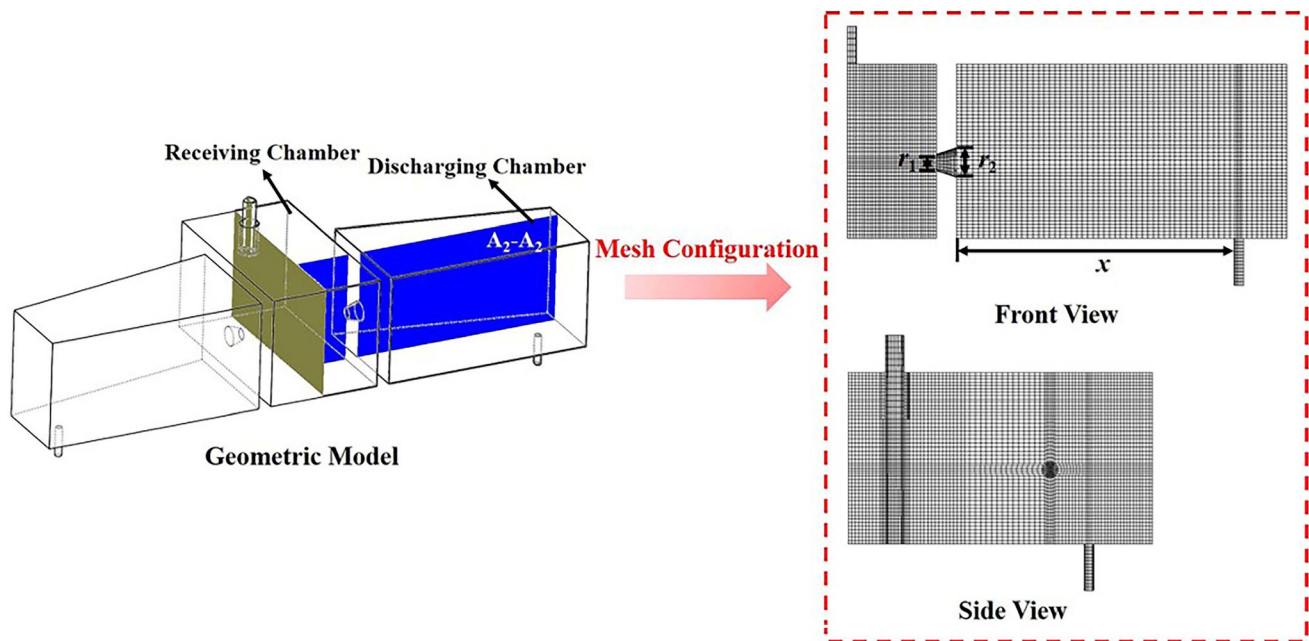
IV. ANALYSIS AND DISCUSSION

A. Fluid Flow and Inclusion Behavior

Figure 7 gives the spatial distribution of inclusion volume concentration and characteristic radius in the single-strand tundish, and x represents the distance from the dam to the tundish exit. (1) The inclusion volume concentration is great in the injected fresh molten steel while the size of inclusion is small. (2) Wherever the dam is located, the inclusion always grows up along the flow path of the fluid because of collision-coalescence among



(a) Single-strand tundish



(b) Two-strand tundish

Fig. 2—Geometric model and mesh configuration.

Table II. Geometry Size of the Tundish

Parameters	Single-Strand Tundish	Multi-Strand Tundish
Length (mm)	1500	4716
Width (mm)	300	1636
Depth of the Liquid Pool (mm)	250	925
Diameter of the Ladle Shroud (mm)	30	100
Diameter of the Outlet (mm)	10	50
Distance Between the Two Outlets (mm)	—	4200
Diameter of the Cone-Shaped Hole (mm)	—	$r_1 = 70, 90/r_2 = 100, 140, 160$

Table III. Physical Properties

Parameter	Value
Steel Grade	200 series stainless steel
Density of Molten Steel (kg/m^3)	7020
Viscosity of Molten Steel (Pa s)	0.0067
Inclusion Composition	MnO (62.99 pct), SiO_2 (19.21 pct), CaO (11.85 pct), Al_2O_3 (5.91 pct), MgO (0.04 pct)
Density of Inclusion (kg/m^3)	4413
Inlet Velocity (m/s)	0.54 (single-strand)/0.81 (two-strand)

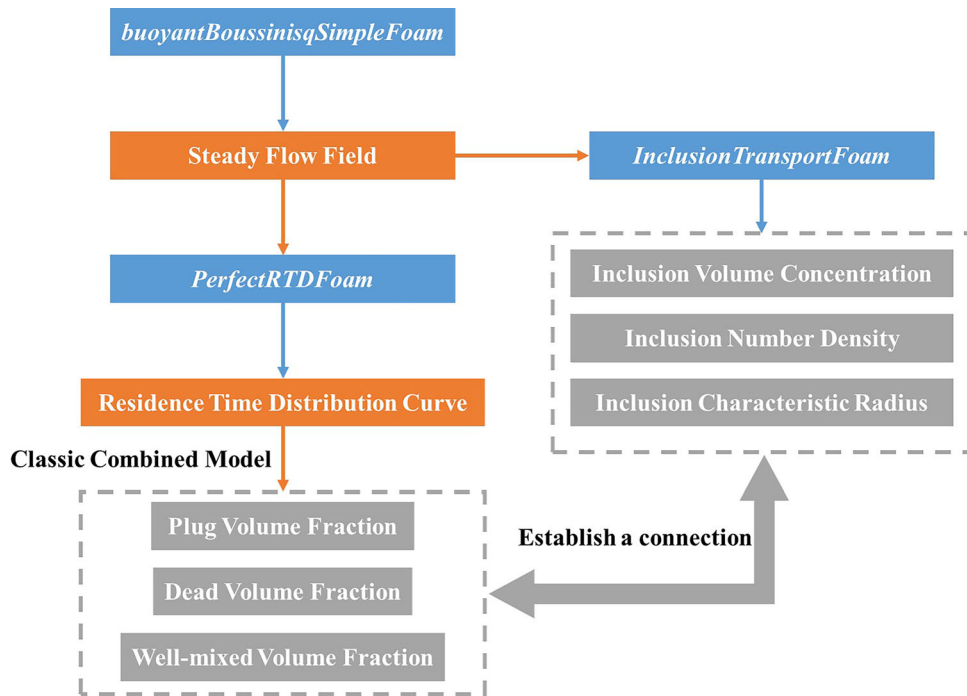


Fig. 3—Numerical procedure for the present research.

inclusions. (3) When the distance from the dam to the tundish exit are 650 and 750 mm, there is a vortex between the dam and the outlet, and the characteristic radius of the inclusion increases because the vortex promotes the collision-coalescence among inclusions. (4) The inclusions follow the molten steel flow because the inclusion particle is small.

Figure 8 shows that the molten steel flow stream and inclusion spatial distribution in the case of different baffle locations and different guide hole sizes. As the baffle is closer to tundish exit, the bigger receiving chamber leads to the stronger vortex. In this way, there are bigger inclusions in the center of the vortex. As the guide hole becomes smaller, the faster molten steel flow in guide hole results in a stronger turbulence. Therefore, inclusions don't have enough time to collide and float up, so the inclusion volume concentration is greater and the characteristic radius is smaller in the discharging chamber.

Figure 8 also shows an interesting phenomenon that there are bigger inclusions with lower volume concentration in the recirculation zone. Following reasons lead to the phenomenon. (1) The recirculation zone in the discharging chamber is bigger than that in the receiving chamber, so inclusions have more time to carry out the collision-coalescence in the discharging chamber. Consequently, the inclusion volume concentration and inclusion characteristic radius are distributed evenly in the receiving chamber. (2) The inclusions can be trapped by the slag and the refractory, thus the inclusion volume concentration is low near the top slag and the refractory wall.

B. Residence Time Distribution Curve Character

Figure 9 shows that RTD curves have different characteristic times and different curve shapes in the case of different control parameters, the related analysis on RTD curve can be found in Figure 10. For the

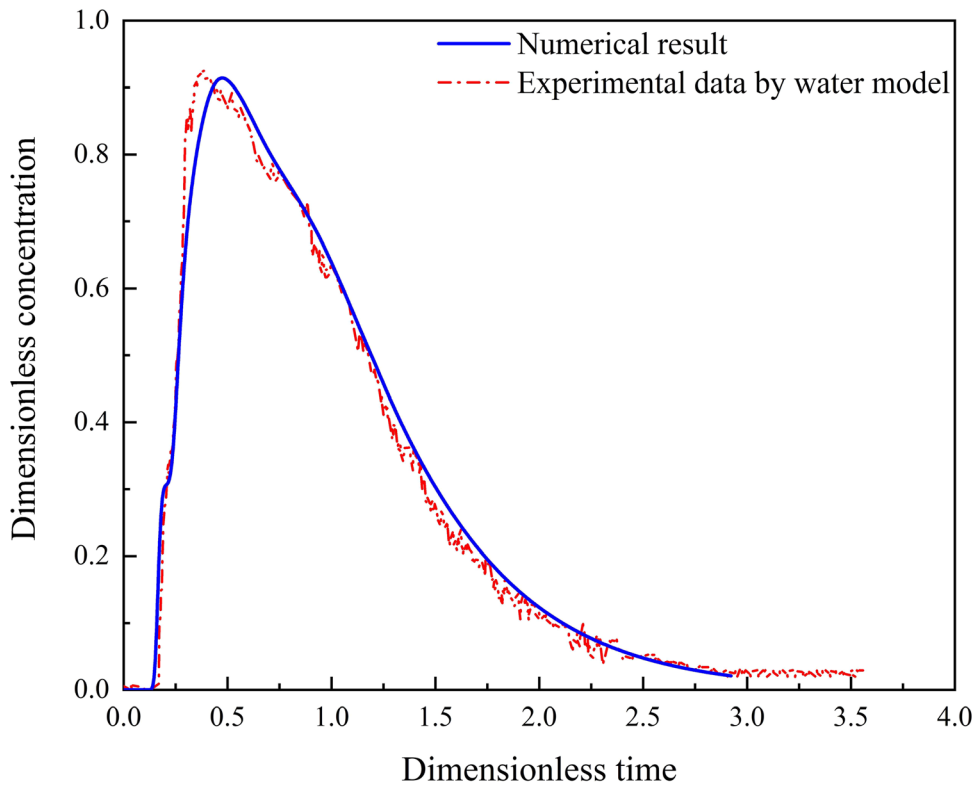


Fig. 4—Comparison of the RTD curves of water model experiment and numerical simulation.

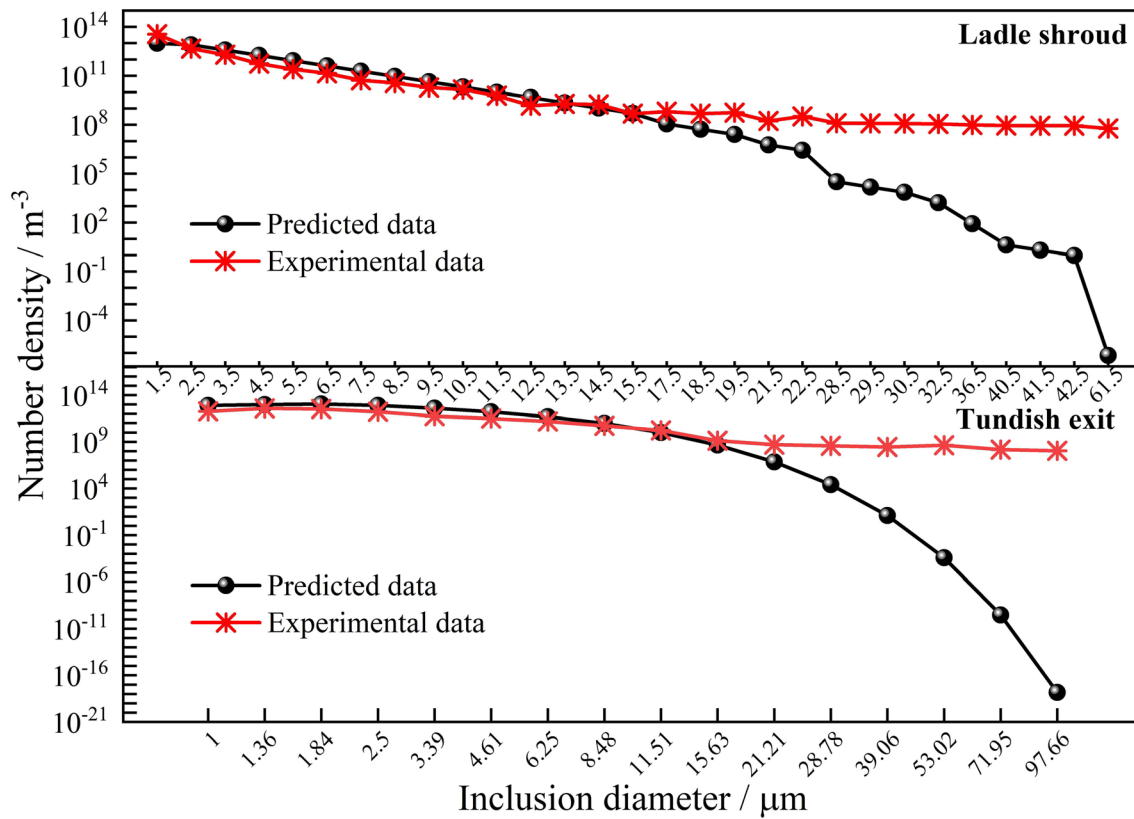


Fig. 5—Comparison of Inclusion number density and inclusion diameter of numerical simulation and industrial measurement.

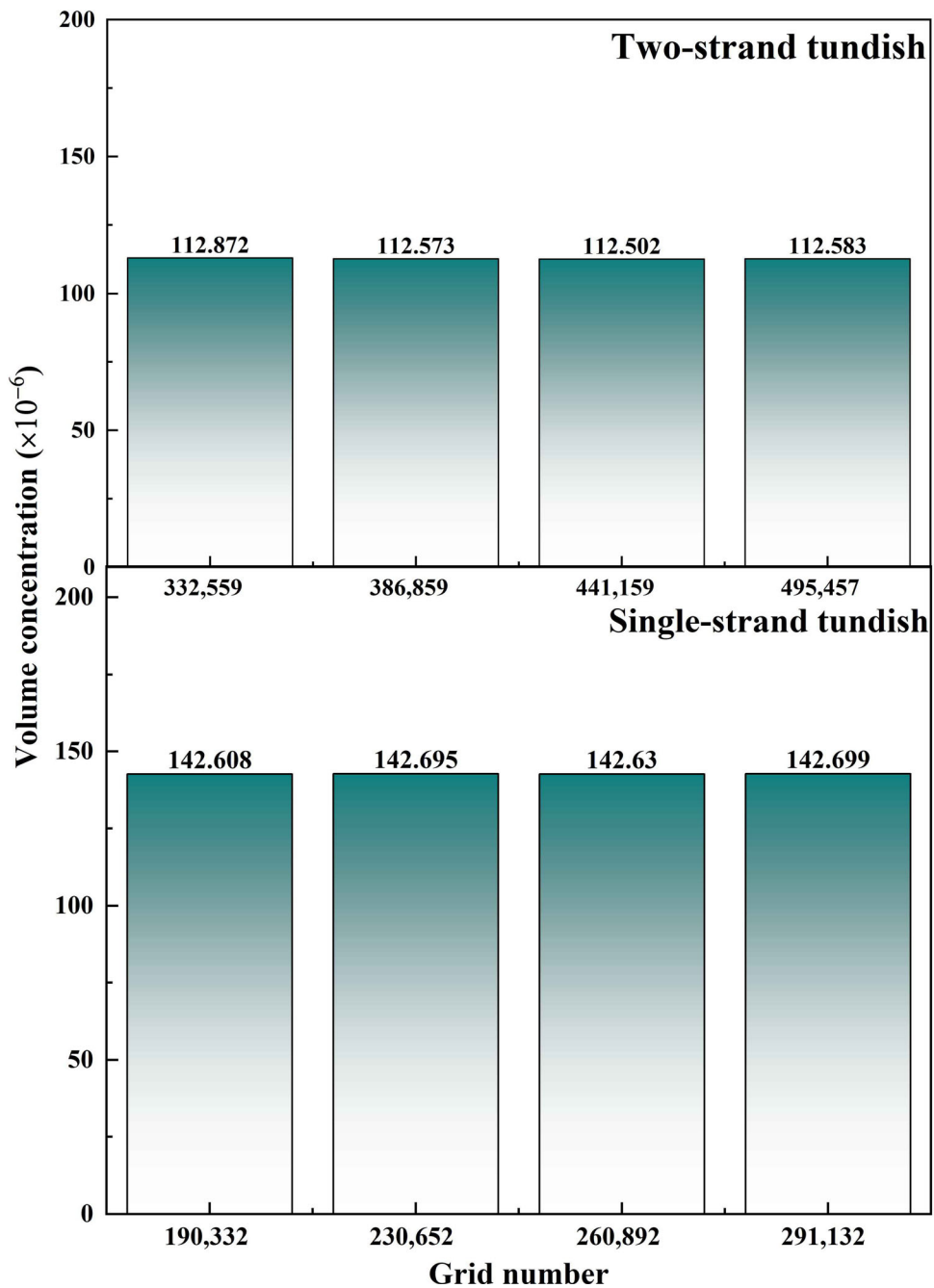
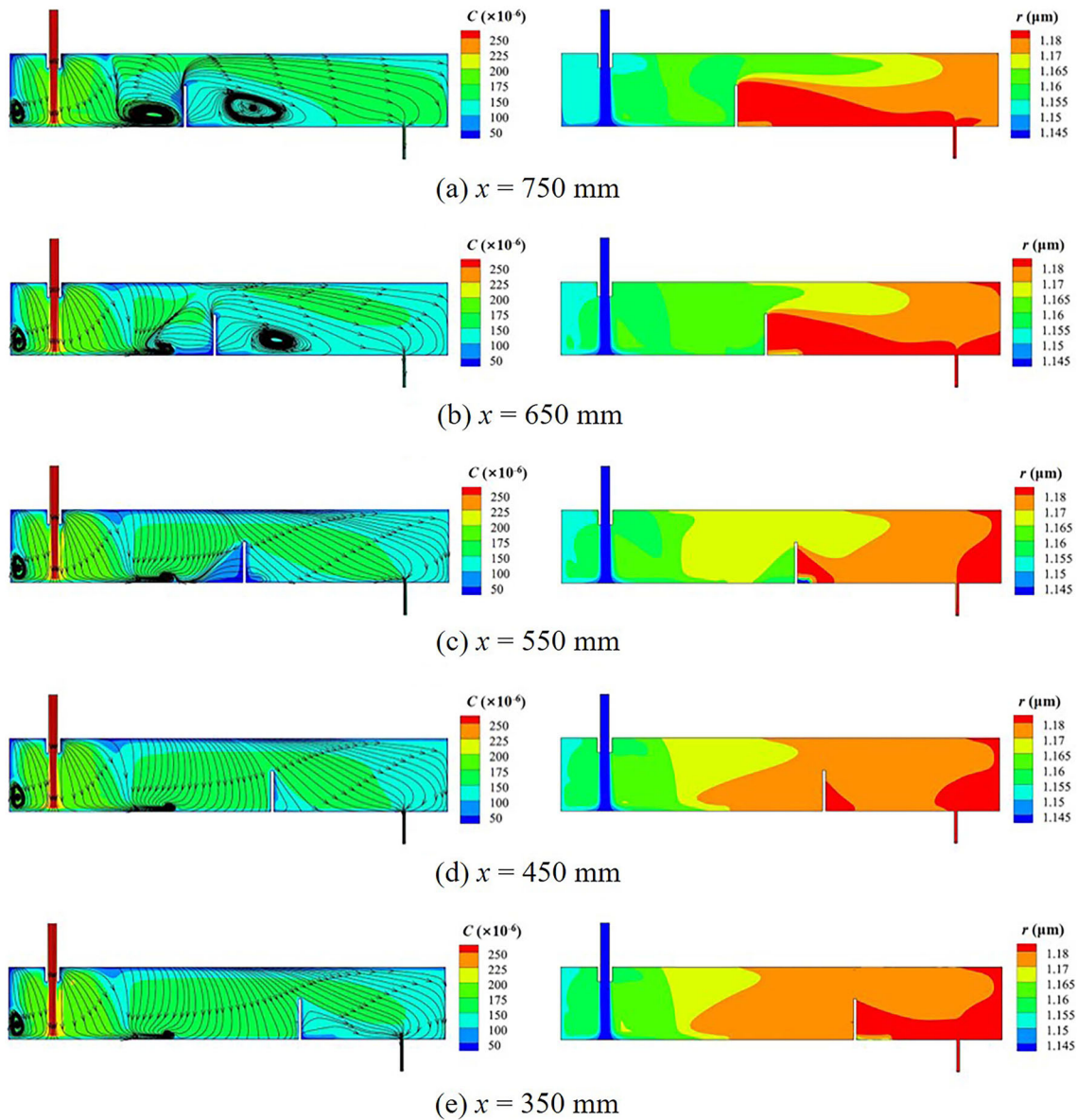


Fig. 6—Grid Independence Verification.

single-strand tundish, with the decrease of the distance between the dam and the tundish exit, the volume fraction of dead zone decreases from 3.58 to 1.42 pct gradually. The volume fraction of plug zone increases from 30.10 to 35.54 pct, then decreases to 32.31 pct. And the volume fraction of well-mixed zone decreases from 66.32 to 62.55 pct, then increases to 66.27 pct. For the two-strand tundish, as the baffle approaching tundish exit, the volume fraction of dead zone gradually

decreases from 15.99 to 13.06 pct; the volume fraction of plug zone increases from 19.09 to 25.83 pct; the volume fraction of well-mixed zone decreases from 64.92 to 61.11 pct. With the decrease of the diameter of the guide hole, the volume fraction of dead zone gradually decreases from 14.16 to 13.73 pct; the volume fraction of plug zone increases from 23.05 to 24.11 pct; the volume fraction of well-mixed zone decreases from 62.79 to 62.16 pct.



Volume concentration

Characteristic radius

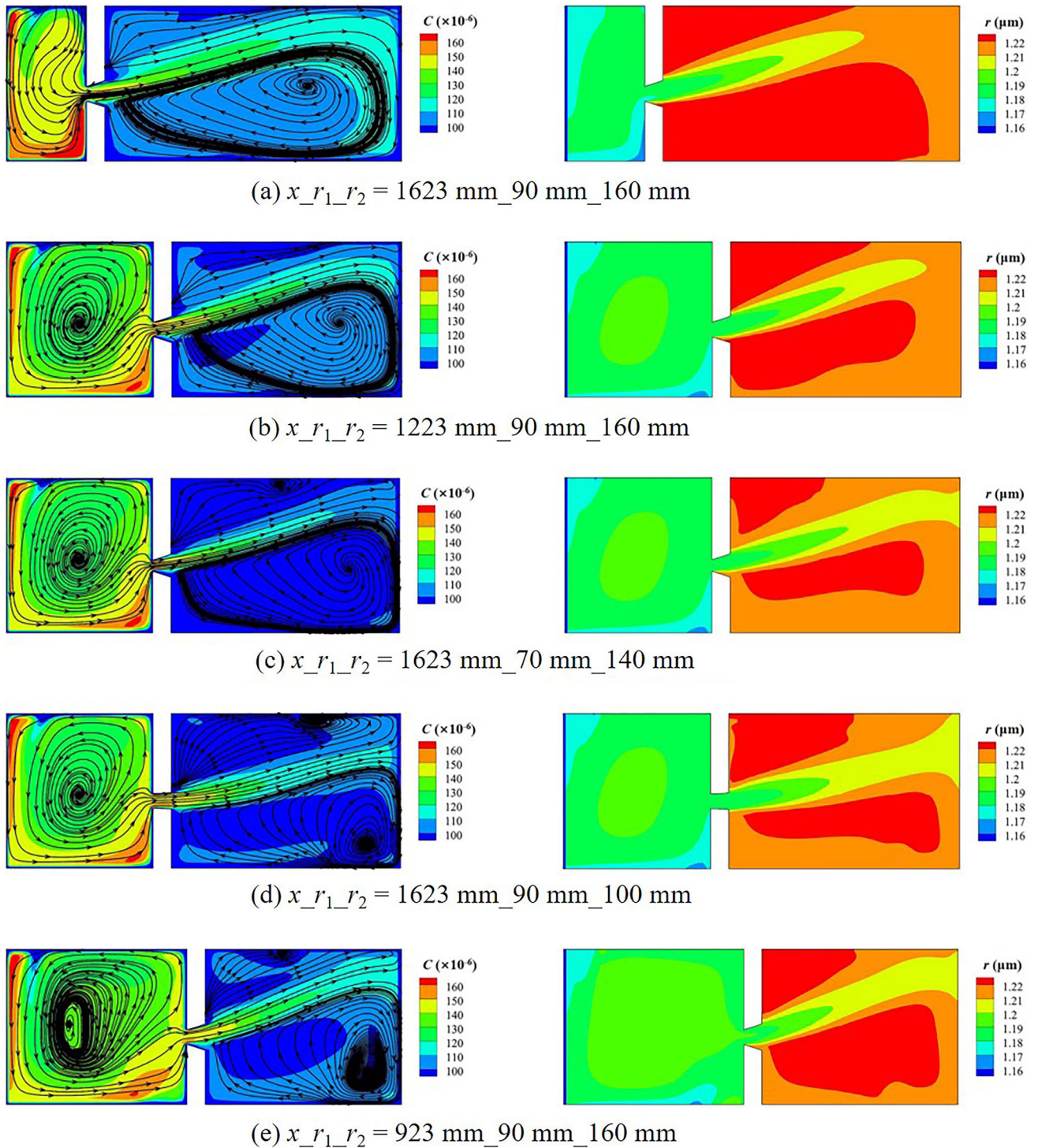
Fig. 7—Inclusion spatial distribution in the case of single-strand tundish for A_1 to A_1 section.

Figure 11 gives characteristic times of RTD curves under the condition of different control parameters. With the distance between the dam and the tundish exit rises from 350 to 750 mm, the average residence time decreases from 290 to 283 s, the peak concentration time increases from 145 to 162 s, then falls to 133 s under the condition of single-strand tundish. When the distance between the baffle and the tundish exit drops from 1623 to 923 mm, the average residence time and peak concentration time under the condition of two-strand tundish increases from 636 s and 253 to 658 s and 350 s, respectively. When the size of guide hole decreases from ($r_1 = 90$ mm, $r_2 = 160$ mm) to ($r_1 = 90$ mm,

$r_2 = 100$ mm), the average residence time and the peak concentration time rise from 650 s and 315 to 653 s and 334 s, respectively.

C. Relationship Between RTD Curve Analysis and Inclusion Behavior

To have a deep understanding on the relationship between residence time distribution curve and inclusion removal rate, the dimensionless inclusion volume concentration (C_{exit}/C_0) is introduced to reveal the inclusion removal rate ($1 - C_{\text{exit}}/C_0$) of the tundish, C_{exit} is the inclusion volume concentration at the tundish outlet, C_0 is the inclusion volume concentration at the tundish



Volume concentration

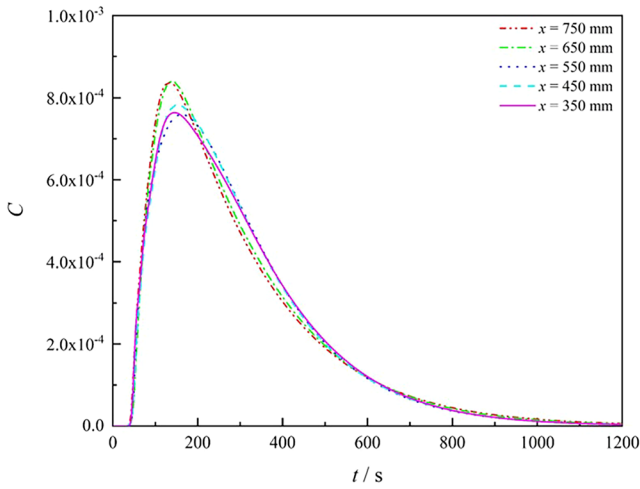
Characteristic radius

Fig. 8—Inclusion spatial distribution in the case of two-strand tundish for A_2 to A_2 section.

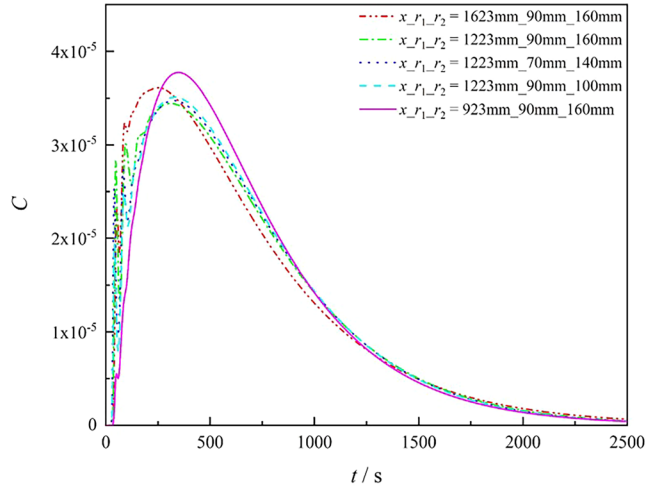
inlet. Figure 12 indicates the following features for the relationship between RTD curve analysis and dimensionless volume concentration:

- (1) As the dead volume fraction decreases from 3.579 to 1.421 pct, the dimensionless inclusion volume concentration drops from 0.489 to 0.468 under the

condition of single-strand tundish. Such a phenomenon can be explained by the factor that the active zone volume (plug volume and well-mixed volume) promotes the inclusion collision-coalescence and removal. However, the inclusion removal rate does not vary monotonically with the dead

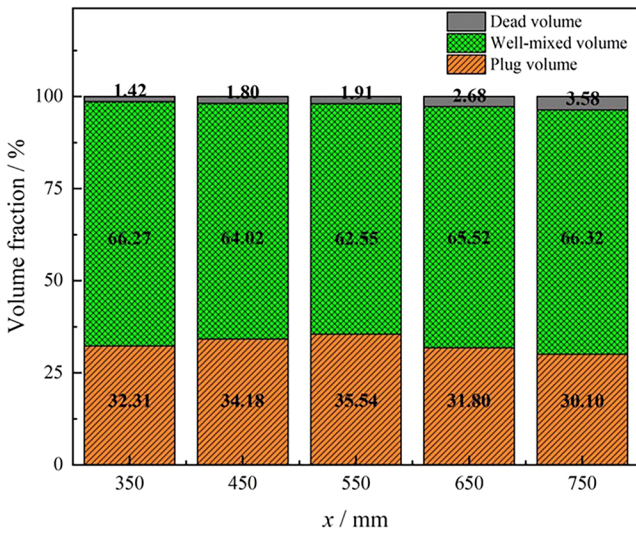


(a) Single-strand tundish

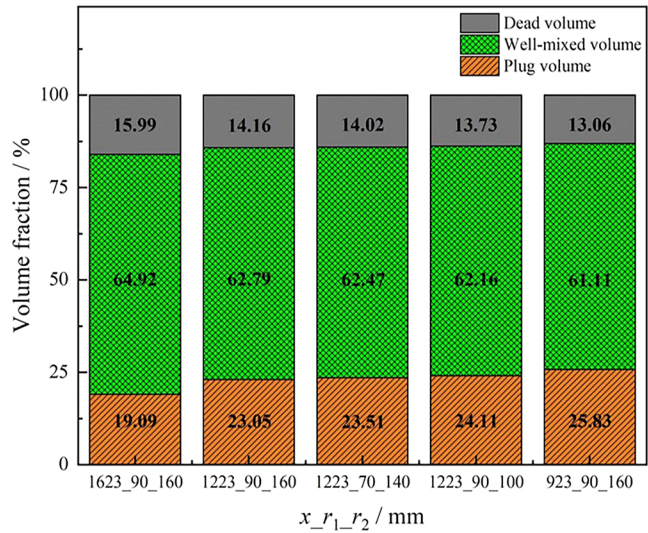


(b) Two-strand tundish

Fig. 9—RTD curves in the tundish with different control parameters.



(a) Single-strand tundish



(b) Two-strand tundish

Fig. 10—RTD curve analysis results in the case of different control parameters.

volume because the dimensionless inclusion volume concentration decrease from 0.3719 to 0.3171, then increases to 0.3426 under the condition of two-strand tundish. Moreover, the inclusion removal rate increases first and then decreases with the increase of dead volume for the two-strand tundish, the increasing trend of dead volume in the case of single-strand tundish may correspond to the inclusion removal rate decreasing trend in the case of two-strand tundish.

(2) As the plug volume fraction and well-mixed volume fraction increase, the dimensionless inclusion volume concentration does not increase (or decrease) monotonically because the inclusion removal is influenced by two factors: collision-coalescence and floating up.

(3) As the ratio of plug volume to dead volume and the ratio of well-mixed volume to dead volume increases from 8.411 to 22.740 and 18.529 to 46.633, the dimensionless inclusion volume concentration drops from 0.489 to 0.468 under the condition of single-strand tundish. The results confirm the points that plug volume prompts the inclusion removal by floating up, and well-mixed volume promotes better colliding and aggregating among the inclusions. However, for the two-strand tundish, when the ratio of plug volume to dead volume and the ratio of well-mixed volume to dead volume increases from 1.194 to 1.678 and from 4.059 to 4.457, the dimensionless inclusion volume concentration drops from 0.372 to 0.317, then increases to 0.3426. The result also indicates inclusion removal rate does not vary

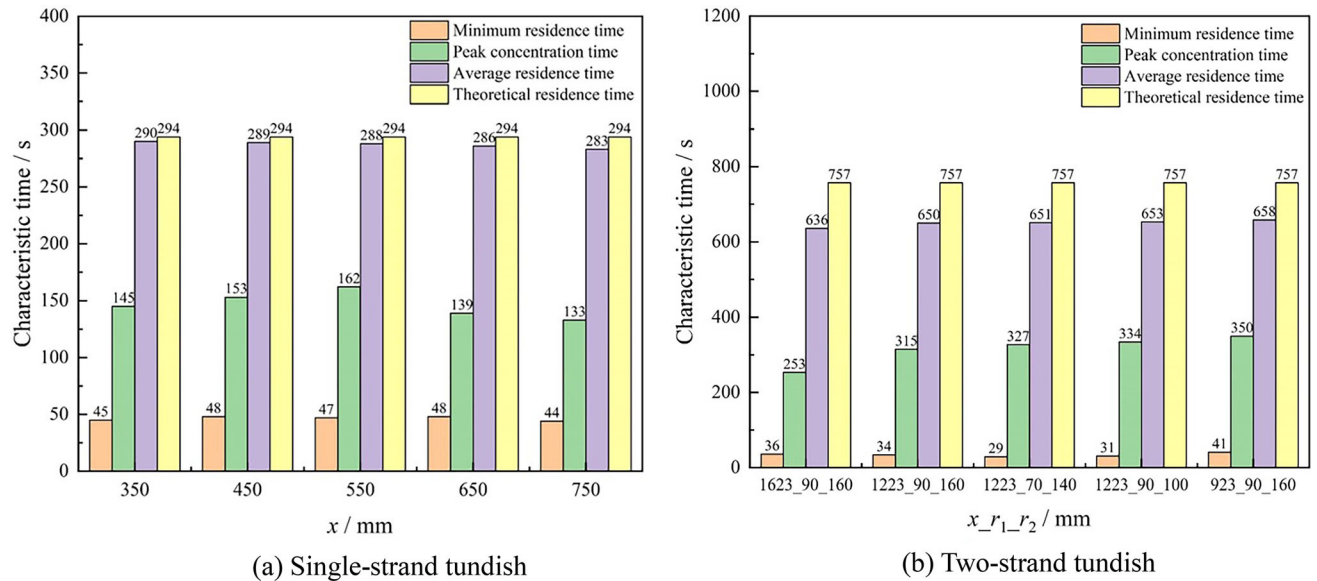


Fig. 11—Characteristic times in the tundish with different control parameters.

monotonically with the plug volume or the well-mixed volume.

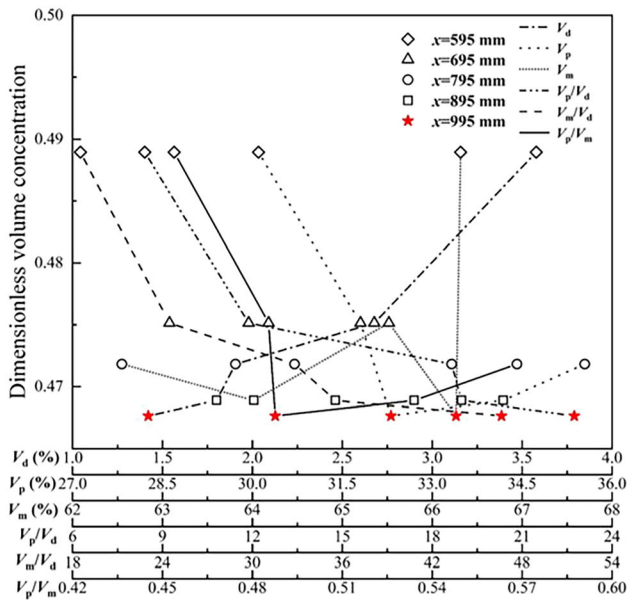
- (4) For the single-strand tundish, as the ratio of plug volume to well-mixed volume (V_p/V_m) increases from 0.454 to 0.568, the dimensionless inclusion volume concentration drops from 0.489 to 0.468, then increases to 0.472. For the two-strand tundish, as the ratio of plug volume to well-mixed volume (V_p/V_m) increases from 0.294 to 0.423, the dimensionless inclusion volume concentration drops from 0.372 to 0.317, then increases to 0.343. In a word, when the ratio of plug volume to well-mixed volume is 0.488, the inclusion removal rate reaches the maximum (53.24 pct) in the case of single-strand tundish. When the ratio of plug volume to well-mixed volume is 0.376, the inclusion removal rate reaches the maximum (68.29 pct) under the condition of the two-strand tundish.

Similar to dimensionless inclusion volume concentration, the dimensionless inclusion characteristic radius (r_{exit}^*/r_0^*) is also introduced to reveal the inclusion size change in the tundish, r_{exit}^* is the inclusion characteristic radius at the tundish exit, r_0^* is the inclusion characteristic radius at the tundish inlet. Figure 13 indicates the following features for the relationship between RTD curve analysis and dimensionless characteristic radius:

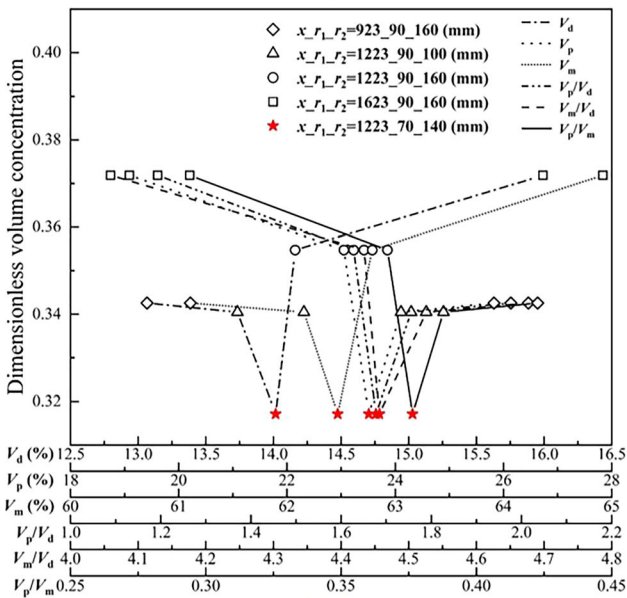
- (1) When the dead volume fraction decreases from 3.579 to 1.421 pct, the dimensionless inclusion characteristic radius increases from 1.042 to 1.045 in the case of single-strand tundish. Such a phenomenon results from the following factor: The increasing active zone volume (plug volume and well-mixed volume) promotes the inclusion collision-coalescence. However, when the dead volume fraction decreases from 15.99 to 13.06 pct under the condition of two-strand tundish, the dimensionless

inclusion characteristic radius decrease from 1.076 to 1.072, then increases to 1.079. Because the non-monotonic relationship between the dead volume and dimensionless inclusion volume concentration.

- (2) When the plug volume fraction and well-mixed volume fraction increase, the dimensionless inclusion characteristic radius does not increase (or decrease) monotonically. Such a phenomenon is similar to the dimensionless inclusion volume concentration.
- (3) When the ratio of plug volume to dead volume and the ratio of well-mixed volume to dead volume increases from 8.411 to 22.740 and 18.529 to 46.633 under the condition of single-strand tundish, the dimensionless inclusion characteristic radius rises from 1.042 to 1.045. However, when the ratio of plug volume to dead volume and ratio of well-mixed volume to dead volume increases from 1.194 to 1.678 and 4.059 to 4.457 under the condition of two-strand tundish, the dimensionless inclusion characteristic radius drops from 1.076 to 1.072, then increases to 1.079.
- (4) When the ratio of plug volume to well-mixed volume is 0.488, the dimensionless inclusion characteristic radius reaches the maximum (1.045) under the condition of the single-strand tundish. When the ratio of plug volume to well-mixed volume is 0.376, the dimensionless inclusion characteristic radius reaches the minimum (1.072) in the case of the two-strand tundish. In other word. When the inclusion removal rate reaches the maximum, the inclusion size reaches the extremum at the tundish exit. But the inclusion extreme size may be the maximum size or the minimum size. It depends on the tundish structure.



(a) Single-strand tundish



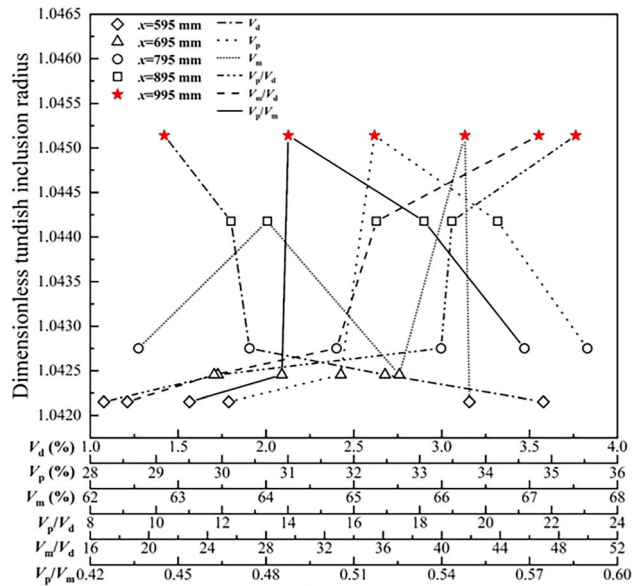
(b) Two-strand tundish

Fig. 12—Relationship between RTD curve analysis and dimensionless volume concentration.

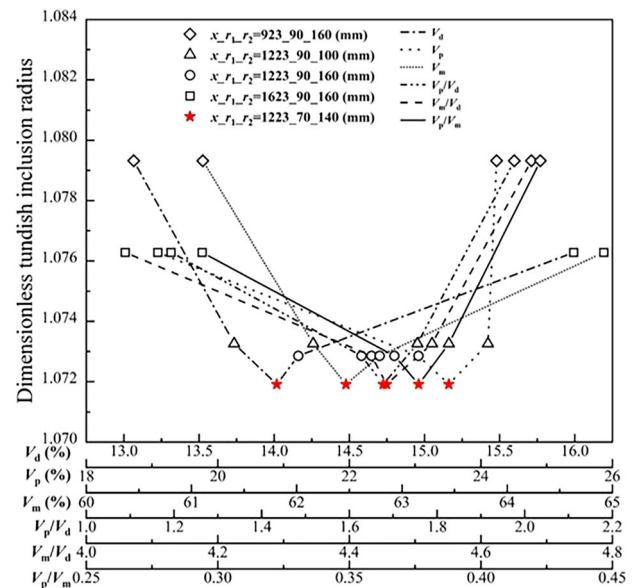
D. Correlation Degree Between RTD Curve and Inclusion Behavior

It is an effective method for Pearson correlation to investigate the correlation degree between two variables.^[39–41] The influence degree $-1 \leq r \leq 1$ ranks the inter-correlations among variables, which is calculated by Eq. [23]. $|r| > 0.5$ means a significant correlation between two variables.

$$r = \frac{\sum_{i=1}^n (x_i - \bar{x})(y_i - \bar{y})}{\sqrt{\sum_{i=1}^n (x_i - \bar{x})^2} \sqrt{\sum_{i=1}^n (y_i - \bar{y})^2}} \quad [23]$$



(a) Single-strand tundish



(b) Two-strand tundish

Fig. 13—Relationship between RTD curve analysis and dimensionless tundish inclusion radius.

Figure 14 gives the correlation degree between RTD curve and inclusion removal rate. There are several interesting results. (1) Compared to the plug volume fraction and the well-mixed volume fraction (V_p , V_m , V_p/V_m), the dead volume fraction (V_d , V_p/V_d , V_m/V_d) is the most important factor to affect the inclusion removal rate under the condition of single-strand tundish, and the influence degree $|r|$ is up to 0.9694 for V_d . (2) The influence degrees $|r|$ are 0.6550 for V_p , 0.6514 for V_d and 0.6586 for V_m under the condition of two-strand tundish. And these values are close to each other. (3) Tanks-in-Series model is applied to divide the two-strand tundish into the receiving chamber and the discharging chamber.^[18] Similar to single-strand

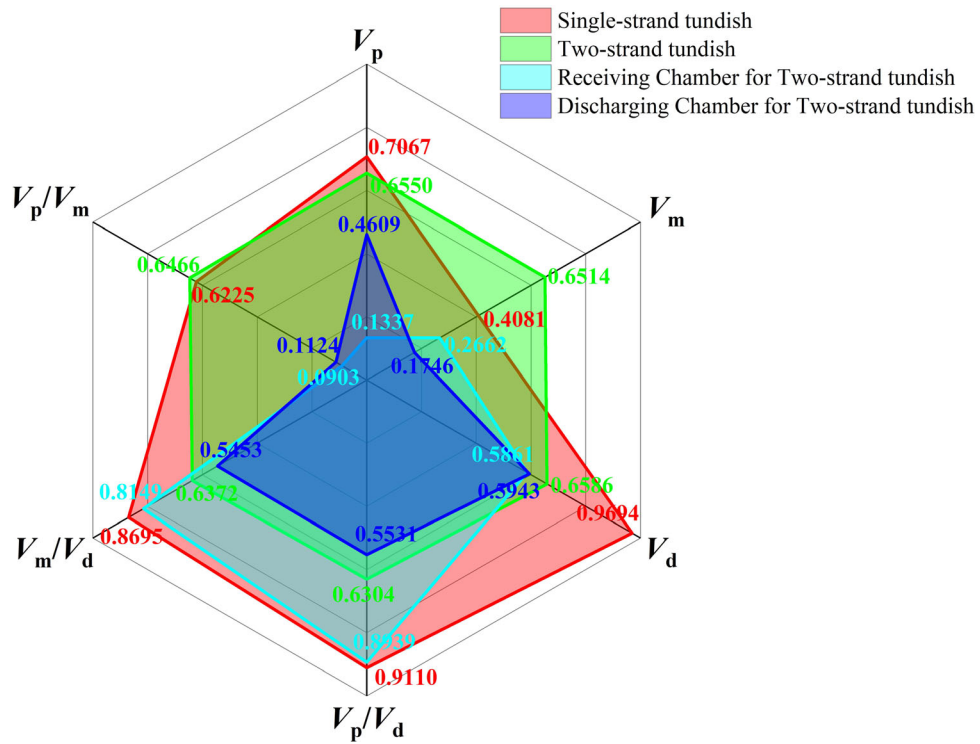


Fig. 14—Correlation degree between RTD curve and inclusion removal rate.

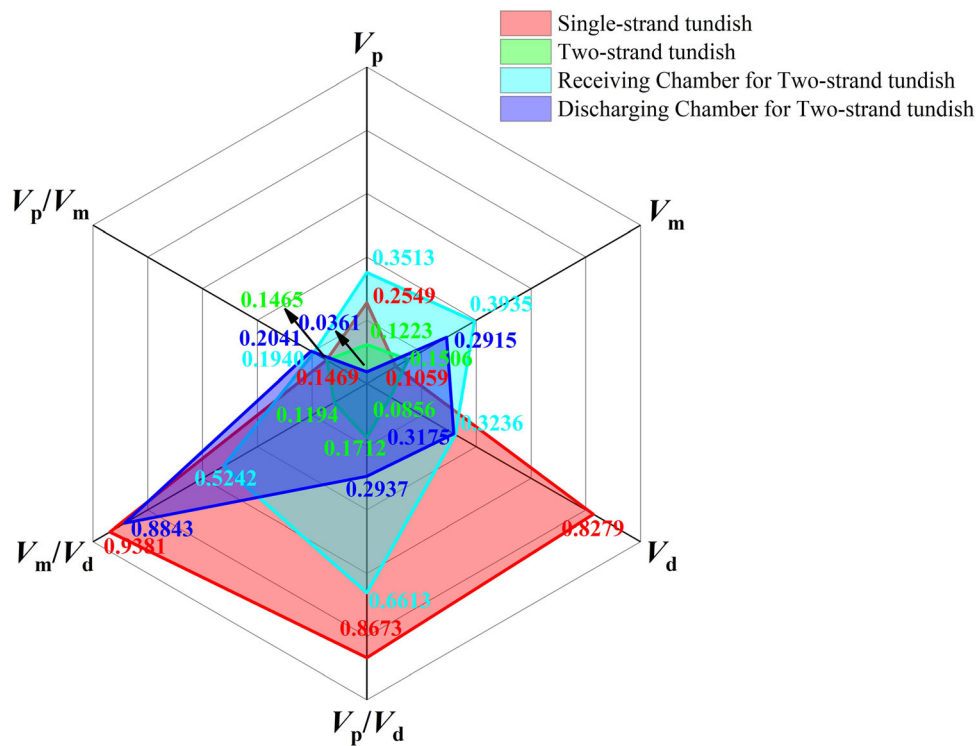


Fig. 15—Correlation degree between RTD curve and dimensionless inclusion characteristic radius.

tundish, the dead volume fraction (V_d , V_p/V_d , V_m/V_d) is the most important factor to affect the inclusion removal rate in the case of the receiving chamber and

the discharging chamber. Furthermore, the influence degrees $|r|$ are up to 0.8939 for V_p/V_d in the receiving chamber, and 0.5943 for V_d in the discharging chamber.

Figure 15 gives the correlation degree between RTD curve and dimensionless inclusion characteristic radius (r_{exit}^*/r_{inlet}^*). There are several interesting results. (1) Similar to the inclusion removal rate, the dead volume fraction (V_d , V_p/V_d , V_m/V_d) is the most important factor to affect the dimensionless inclusion characteristic radius under the condition of single-strand tundish, and the influence degree $|r|$ is up to 0.9381 for V_m/V_d . (2) The influence degrees $|r|$ are relatively small ($|r| < 0.2$) for V_p , V_m , V_d and for their ratio of the above volume fractions (V_p/V_d and V_m/V_d) under the condition of two-strand tundish. And the greatest influence factor $|r|$ is only 0.1712 for V_p/V_d . (3) In the receiving chamber of the two-strand tundish, the influence degrees of V_p , V_m , and V_d on the dimensionless characteristic radius are close to each other. However, the influence degree is significantly increased ($|r| > 0.5$) for V_p/V_d and V_m/V_d . (4) In the discharging chamber of the two-strand tundish, the ratio of well mixed volume fraction to dead volume fraction ($V_m/V_d = 0.8843$) is the most important factor to affect the dimensionless inclusion characteristic radius.

V. CONCLUSIONS

Turbulent flow is the key factor of inclusion behavior in tundish. The residence time distribution curve is widely used to analyze flow field. The inclusion mass/population conservation model is applied to describe the inclusion behavior in tundish. The following conclusions can be summarized.

- (1) Whatever it is the single-strand tundish or the two-strand tundish, shortening the distance between the baffle or the dam and the tundish exit or narrowing the size of guide hole can reduce the dead volume in the tundish.
- (2) The dimensionless inclusion characteristic radius and the inclusion removal rate do not vary monotonically with plug volume fraction, well-mixed volume fraction or dead volume fraction.
- (3) A lower dead volume fraction is not the only criterion for better inclusion removal performance. For the same control devices in a tundish, structure parameters (distance between dam/baffle to tundish exit, the diameter of the hole in the baffle) can be optimized to obtain the maximum inclusion removal rate. Such a critical state can be expressed by the ratio of plug volume fraction to well-mixed volume fraction (V_p/V_d). But the dimensionless inclusion characteristic radius may be the maximum or the minimum at this critical state.
- (4) Among plug volume fraction, well-mixed volume fraction and dead volume fraction, dead volume fraction is the most important factor to affect the dimensionless inclusion characteristic radius and the inclusion removal rate.

ACKNOWLEDGMENTS

The research is supported by the Fundamental Research Funds for the Central Universities (N2109003).

COMPETING INTEREST

The authors declare that they have no known competing financial interests or personal relationships that could have appeared to influence the work reported in this paper.

REFERENCES

1. M.J. Zhao, Y. Wang, S.F. Yang, J.S. Li, W. Liu, and Z.Q. Song: *J. Mater. Res. Technol.*, 2021, vol. 13, pp. 561–72.
2. M.J. Zhao, Y. Wang, S.F. Yang, M.L. Ye, J.S. Li, and Y.H. Liu: *Metals*, 2021, vol. 11, p. 722.
3. H. Zhang, H. Lei, C.Y. Ding, S.F. Chen, H. Niu, and B. Yang: *Steel Res. Int.*, 2022, vol. 93, p. 2200181.
4. B. Yang, K. Liu, H. Lei, and P. Han: *High Temp. Mater. Process.*, 2022, vol. 41, pp. 460–68.
5. S. Chang, Z.S. Zou, J.H. Liu, M. Isac, X.K.E. Cao, X.F. Su, and R.I.L. Guthrie: *Powder Technol.*, 2021, vol. 387, pp. 125–35.
6. S. Chang, W.X. Huang, Z.S. Zou, B.K. Li, and R.I.L. Guthrie: *Powder Technol.*, 2020, vol. 367, pp. 296–304.
7. C. Yao, M. Wang, H.H. Zhu, L.D. Xing, and Y.P. Bao: *Metall. Mater. Trans. B*, 2023, vol. 54B, pp. 1144–58.
8. J.H. Wang, Q. Fang, L. Huang, P. Zhao, X.Q. Xie, and H. Zhang: *Metall. Mater. Trans. B*, 2023, vol. 54B, pp. 635–49.
9. Y. Sahai and R.J.I. Ahuja: *Ironmak. Steelmak.*, 1986, vol. 13, pp. 241–47.
10. Y. Sahai and T. Emi: *ISIJ Int.*, 1996, vol. 36, pp. 667–72.
11. Q. Wang, Y. Liu, A. Huang, W. Yan, H.Z. Gu, and G.Q. Li: *Metall. Mater. Trans. B*, 2020, vol. 51B, pp. 276–92.
12. W.X. Huang, S. Chang, Z.S. Zou, L. Shao, Y.X. Qu, and B.K. Li: *Steel Res. Int.*, 2021, vol. 92, p. 2100012.
13. S. Chang, L.C. Zhong, and Z.S. Zou: *ISIJ Int.*, 2015, vol. 55, pp. 837–44.
14. Q. Wang, Y. Liu, A. Huang, W. Yan, H.Z. Gu, and G.Q. Li: *Powder Technol.*, 2020, vol. 367, pp. 358–75.
15. Q. Fang, H. Zhang, R.H. Luo, C. Liu, Y. Wang, and H.W. Ni: *J. Mater. Res. Technol.*, 2020, vol. 9, pp. 347–63.
16. H.T. Ling, L.F. Zhang, and H.J. Wang: *Metall. Res. Technol.*, 2017, vol. 114, p. 516.
17. M. Tkadleckova, J. Walek, K. Michalek, and T. Huczala: *Metals*, 2020, vol. 10, p. 849.
18. D.Y. Sheng and Z.S. Zou: *Metals*, 2021, vol. 11, p. 208.
19. C. Liu, A.D. Xiao, Z. He, W. Yan, G.Q. Li, and Q. Wang: *Steel Res. Int.*, 2022, vol. 93, p. 2100818.
20. A.P. Zhang, M.M. Zhu, and J. Luo: *Symposium on Materials Processing Fundamentals at Annual Meeting of The-Minerals-Metals-Materials-Society (TMS)*, Electronic network, March 14–18, 2021. pp. 31–41.
21. J. Luo, S.K. Peng, A.P. Zhang, and Y. Zhong: *Symposium on Materials Processing Fundamentals at Annual Meeting of The-Minerals-Metals-Materials-Society (TMS)*, Electronic network, March 14–18, 2021. pp. 3–12.
22. M.R.M. Yazdi, A.R.F. Khorasani, and S. Talebi: *Can. Metall. Q.*, 2019, vol. 58, pp. 379–88.
23. B. Yang, H. Lei, Q. Bi, Y.Y. Xiao, and Y. Zhao: *JOM*, 2018, vol. 70, pp. 2950–57.
24. H. Lei, L.Z. Wang, Z.N. Wu, and J.F. Fan: *ISIJ Int.*, 2002, vol. 42, pp. 717–25.
25. D.Q. Geng, J.X. Zheng, K. Wang, P. Wang, R.Q. Liang, H.T. Liu, H. Lei, and J.C. He: *Metall. Mater. Trans. B*, 2015, vol. 46B, pp. 1484–93.

26. L.F. Zhang, J. Aoki, and B.G. Thomas: *Metall. Mater. Trans. B*, 2006, vol. 37B, pp. 361–79.
27. H. Lei: *Metall. Mater. Trans. B*, 2015, vol. 46B, pp. 2408–13.
28. C.Y. Ding, H. Lei, S.F. Chen, H. Zhang, Y. Zhao, and Z.S. Zou: *Steel Res. Int.*, 2022, vol. 93, p. 2200187.
29. H. Lei, B. Yang, Q. Bi, Y.Y. Xiao, S.F. Chen, and C.Y. Ding: *ISIJ Int.*, 2019, vol. 59, pp. 1811–19.
30. L.F. Zhang, S. Taniguchi, and K.K. Cai: *Metall. Mater. Trans. B*, 2000, vol. 31B, pp. 253–66.
31. D.Q. Geng, H. Lei, and J.C. He: *ISIJ Int.*, 2010, vol. 50, pp. 1597–605.
32. M.Y. Zhu, S.G. Zheng, Z.Z. Huang, and W.P. Gu: *Steel Res. Int.*, 2005, vol. 76, pp. 718–22.
33. C.Y. Ding, H. Lei, H. Zhang, M. Xu, Y. Zhao, and Q. Li: *J. Mater. Res. Technol.*, 2023, vol. 23, pp. 5400–12.
34. H. Lei, D.Q. Geng, and J.C. He: *ISIJ Int.*, 2009, vol. 49, pp. 1575–82.
35. T. Mizoguchi, Y. Ueshima, M. Sugiyama, and K. Mizukami: *ISIJ Int.*, 2013, vol. 53, pp. 639–47.
36. C.Y. Ding, H. Lei, H. Niu, H. Zhang, B. Yang, and Y. Zhao: *Metals*, 2021, vol. 11, p. 430.
37. C.Y. Ding, H. Lei, H. Niu, H. Zhang, B. Yang, and Q. Li: *Metall. Mater. Trans. B*, 2021, vol. 52B, pp. 3788–804.
38. H.T. Ling, L.F. Zhang, and H. Li: *Metall. Mater. Trans. B*, 2016, vol. 47B, pp. 2991–3012.
39. S.C. Chelgani, S.S. Matin, and S. Makaremi: *Measurement*, 2016, vol. 94, pp. 416–22.
40. S.S. Matin, L. Farahzadi, S. Makaremi, S.C. Chelgani, and G. Sattari: *Appl. Soft Comput.*, 2018, vol. 70, pp. 980–87.
41. M. Jafari, M. Golzadeh, S.Z. Shafaei, H. Abdollahi, M. Gharabaghi, and S.C. Chelgani: *Processes*, 2019, vol. 7, p. 653.

Publisher's Note Springer Nature remains neutral with regard to jurisdictional claims in published maps and institutional affiliations.

Springer Nature or its licensor (e.g. a society or other partner) holds exclusive rights to this article under a publishing agreement with the author(s) or other rightsholder(s); author self-archiving of the accepted manuscript version of this article is solely governed by the terms of such publishing agreement and applicable law.